Biogeochemical Controls on Trace Metal Cycling in Anoxic Marine Sediments

ARTICLE *in* ENVIRONMENTAL SCIENCE AND TECHNOLOGY · DECEMBER 1997

Impact Factor: 5.33 · DOI: 10.1021/es970387e

2 AUTHORS, INCLUDING:

David Craig Cooper
Government of the State of Idaho
24 PUBLICATIONS **481** CITATIONS

Environ. Sci. Technol. **1998**, *32,* 327−330

Biogeochemical Controls on Trace Metal Cycling in Anoxic Marine Sediments

D. CRAIG COOPER* AND JOHN W. MORSE
Department of Oceanography, Texas A&M University, Eller Building, College Station, Texas 77843

The solid phase chemical speciation of Fe, Cu, Ni, and Zn was investigated in two different biogeochemical environments in Chesapeake Bay to quantify the seasonal variability in the concentration of sulfide minerals and associated trace metals in the top 10 cm of sediment. When acid volatile sulfides (AVS) constitute less than 20% of HCl-soluble Fe ("reactive" Fe), the system is dynamic with respect to metals, and the formation and destruction of AVS minerals can potentially result in statistically significant seasonal shifts in both the flux of Cu across the sediment−water interface and the sedimentary concentration of Cu and Zn. When greater than 20% of HCl-soluble Fe is bound within AVS minerals, there is enough sulfide to effectively trap metals within the sediments, and temporal variations in AVS and pyrite do not necessarily result in temporal variations in the concentration of diagenetically available trace metals. Analysis of the ratio of reactive Fe to AVS can potentially increase the reliability of environmental impact predictions.

Introduction

It has long been acknowledged that sulfide minerals play an integral role in controlling trace metal chemistry in anoxic marine environments (*1*−*6*). Although there is a large body of work examining the chemistry of pyrite oxidation in acid mine environments (*7*) and the associated behavior of toxic metals, most of the work done in marine and lacustrine environments has focused on quantifying the processes by which sulfide mineral formation removes trace metals from the aquatic system for subsequent burial with pyrite. Consequently, there has been a general assumption that, within these systems, sulfide mineral formation acts as a permanent sink for many trace metals. Morse (*8*, *9*) demonstrated that up to 90% of estuarine pyrite can oxidize within 1 day of exposure to oxic seawater and release the accompanying trace metals into the "reactive" (HCl-soluble) phase. Cooper and Morse (*10*) noted that the speciation of trace metals and sulfide minerals within the shallow sediments of Offatts Bayou, TX, can change significantly with the seasonal formation and destruction euxinic conditions. This work demonstrates the potential for sulfide-associated trace metals to enter a more bioavailable phase following a major oxidation event (e.g., dredging, storm resuspension, destruction of a shallow euxinic basin) and indicates that oxidative dissolution of sulfide minerals could act as an important source for trace metal fluxes into overlying waters. Here we present the results of a field study designed to examine this possibility.

* Corresponding author tel: (409) 845-9633; fax: (409) 845-9631; e-mail: dcooper@ocean.tamu.edu.

Methods

Sediment box cores were taken in May 1994, July 1994, September 1994, and March 1995 from both site M and site S. Multiple 2.5 in. I.D. subcores were then taken from the single sediment box core and quick-frozen on dry ice for later analysis. Cores for sulfide and metal analysis were thawed in the laboratory and extruded at 2-cm intervals in a glovebag under a high-purity N_2 atmosphere. These samples were sealed in plastic bottles and immediately frozen on dry ice for later analysis. Separate cores were taken for organic and carbonate carbon, porosity, and grain size distribution. These cores were extruded in open air, and the samples were immediately frozen for later analysis. Although multiple cores were taken, only one sediment profile was generated for each parameter at each sampling interval.

Porosity was determined by weight change after drying the sediment for 24 h at 110 °C. Total carbon and organic carbon concentrations were measured on a LECO carbon analyzer (±1% precision), and inorganic carbon was calculated as their difference. Grain size fractions were separated by wet-sieving the sediment through standard sieves. The weight percent dry solids in the less than 62.5-μm fraction is defined as the "fine" (silt + clay) fraction of the sediments. Acid volatile sulfides (AVS) were measured via acid distillation of wet sediment samples using cold 6 N HCl with $SnCl_2$ added and using a potentiometric titration of sulfide with lead perchlorate (*11*). Total reduced inorganic sulfur (TRS) was analyzed by acid distillation with acidic Cr^{2+} followed by potentiometric titration of sulfide with lead perchlorate (*12*). Pyrite sulfur is defined as the difference between total reduced sulfur and acid volatile sulfur.

Iron and trace metal species were analyzed by a sequential extraction procedure (*13*) that is an adaptation of the technique of Lord (*14*) for determining pyrite-Fe. Sediment subsamples were subjected to a sequential series of four leaches; 1 M HCl (reactive fraction), 10 M HF (silicate fraction), 1% NH_4OH (organic fraction), and concentrated HNO_3 (pyrite fraction). Fe and Zn were determined by flame atomic absorption spectrophotometry on a Perkin Elmer 2380 AAS. Precision for these elements was always within 5%. Hg was analyzed spectrophotometrically with a Laboratory Data Control UV monitor equipped with a 30-cm path length cell using the cold vapor technique (*15*). Cu and Ni were determined by Zeeman effect flameless atomic absorption spectrophotometry on a Perkin Elmer 4100 ZL AAS. Precision for the analyses of these elements was always within 10%. All standard solutions were commercially available standards diluted in the respective extraction medium. Calculations were based on standard calibrations, except for rare cases where individual solution matrix effects forced results to be based on the method of standard additions. Detection limits were determined with replicate standards, and all analyses were within detection limits. Acidic working standards were always freshly prepared. All glassware and plasticware were cleaned using established acid leaching procedures.

Interpretation of results is complicated by the need to accurately distinguish between effects that are due to spatial variability and trends that result from temporal changes in the sedimentary environment. Spatial variability at the diffusion-dominated site M was estimated by comparing the values of the measured parameters at a depth beneath the temporally affected zone (12 cm). Spatial variability at this site (based on analyses from three of the four cores collected) was less than or equal to the estimated net analytic and extraction precision for all parameters, and given error bars

S0013-936X(97)00387-8 CCC: $15.00
Published on Web 01/01/1998

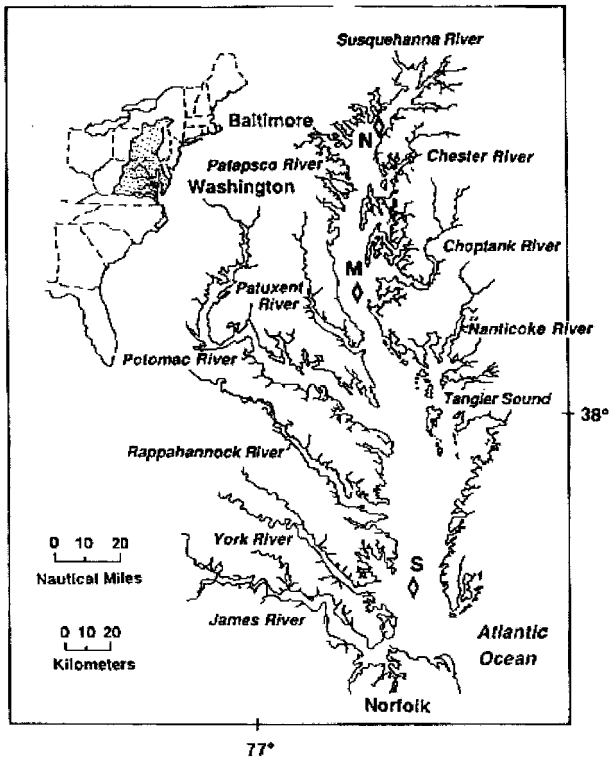

FIGURE 1. Chesapeake Bay sites S and M (*18*).

represent the level of combined net analytic and extraction uncertainty. The effect of spatial variability is more difficult to quantify at the heavily bioturbated site S. Variability in the degree of bioturbation will result in a larger degree of lateral heterogeneity at site S than at site M, and the depth dependence of bioturbation precludes the use of samples from deeper depths to estimate the degree of lateral heterogeneity in surficial sediments. Data presented by Marvin-DiPasquale and Capone (*16*) indicate that spatial variability in the upper 2 cm of sediments from the lower Chesapeake Bay varies between approximately 10% (POC/PON ratio, SO_4^{2-} concentration) and 30% (integrated SO_4 reduction rate), depending upon the parameter measured. Furthermore, both site M and site S display a strong temporal trend in DOC flux (*17*), $\sum CO_2$ flux (*17*), integrated SO_4 reduction rate (*16*), and bottom water temperature (*16*, *17*). While this approach does not allow strong quantification of the degree of lateral heterogeneity, it does indicate that temporal changes in Chesapeake Bay are of much greater magnitude than simple lateral heterogeneity. Given error bars for site S reflect the degree of net analytic and extraction uncertainty and are in good agreement with the results from previously reported research (*16*, *18*).

Results

Chesapeake Bay sites S and M (Figure 1) are located in an open bay system that is representative of coastal plain estuaries. Other researchers (*17*, *18*) have examined the pore water biogeochemistry and sediment carbon budget of these sites and noted that $\sum CO_2$ and DOC fluxes are lower at the heavily bioturbated site S than at site M where transport is dominated by molecular diffusion (*18*). Skrabal and Donat (*17*) observed that, although the flux of Cu-complexing ligands increased from 320 ± 80 nmol m^{-2} d^{-1} to 1200 ± 170 nmol m^{-2} d^{-1} from March to July 1995, the flux of total dissolved Cu from site M sediments did not display a corresponding change (53 ± 17 nmol m^{-2} d^{-1} in March; 30 ± 10 nmol m^{-2} d^{-1} in July). The flux of Cu-complexing ligands remained constant at site S (440 ± 160 nmol m^{-2} d^{-1} in March; 420 ± 95 nmol m^{-2} d^{-1} in July), while the flux of total dissolved Cu increased from 11 ± 4 nmol m^{-2} d^{-1} in March to 85 ± 25 nmol m^{-2} d^{-1} in July (*17*). We have observed corresponding differences in the solid phase geochemistry of these sites and present evidence that several easily measured parameters are indicative of the fundamental geochemical processes that control the aqueous concentration and potential bioavailability of many trace metals.

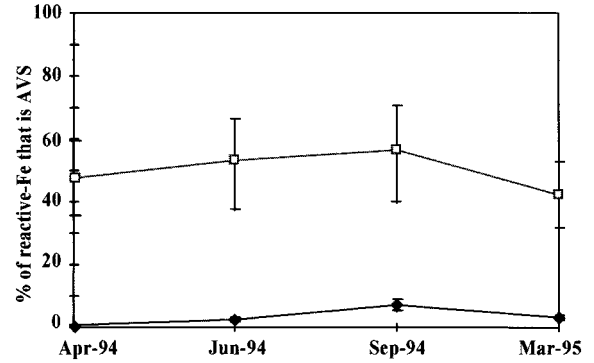

FIGURE 2. Average (top 10 cm) percentage of HCl iron that is associated with AVS minerals (AVS/HCl-Fe) × 100, at site M (open squares) and site S (solid circles).

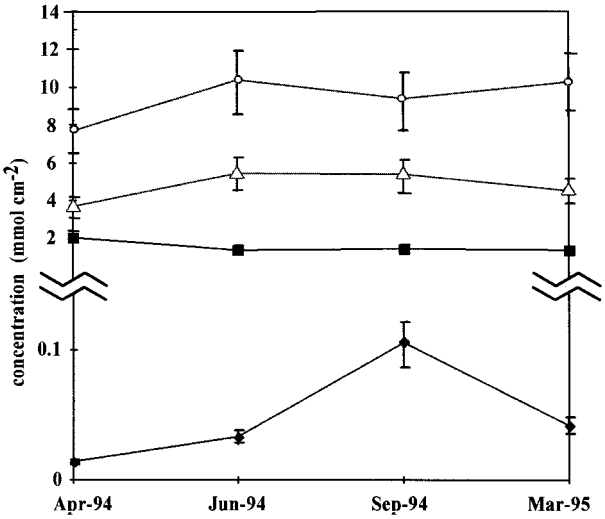

FIGURE 3. Integrated mass (top 10 cm) of AVS (open triangles, solid diamonds) and HCl-Fe (open circles, solid squares) at site M (open symbols) and site S (solid symbols). Note the change in scale.

Site S (water depth ~10 m) is located in the southern portion of Chesapeake Bay where bottom waters are oxygenated year-round (*18*), and it is representative of an iron-dominated environment. Depth-integrated (top 10 cm) AVS did not exceed 0.1 mmol cm^{-2}, and pyrite-S did not exceed 2 mmol cm^{-2}. The sediments were coarse-grained (porosity ~0.5), organic carbon comprised less than 0.5% of total sediment mass, and less than 10% of the HCl-extractable iron was associated with AVS minerals.

Published data has demonstrated a strong seasonal trend in bottom water temperature and sulfate reduction rate at site S (*16*, *18*) and provides support for our observation that depth integrated AVS (Figure 3) increased 3-fold from July to October 1994 followed by a subsequent decrease back to the initial value of approximately 0.03 mmol cm^{-2} by mid-March 1995. A similar trend was seen in the proportion of reactive iron that is bound within AVS minerals (Figure 2). Pyrite-S, pyrite-Fe (Figure 4), and reactive-Fe (Figure 3) did not vary appreciably with season. The mass of HCl plus HNO_3 Cu (Figure 5) and Zn (Figure 6) increased more than 2-fold from July to October and then decreased back to the

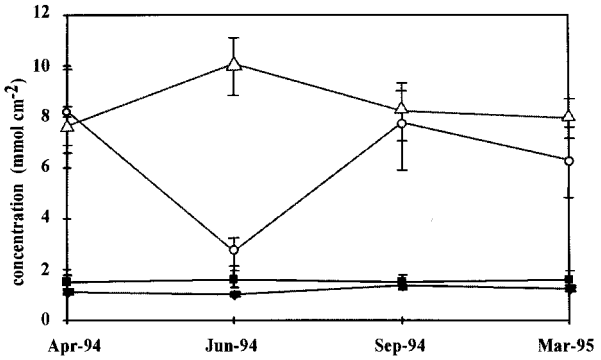

FIGURE 4. Integrated mass (top 10 cm) of pyrite-S (open triangles, solid diamonds) and 2HNO_3-Fe (open circles, solid squares) at site M (open symbols) and site S (solid symbols).

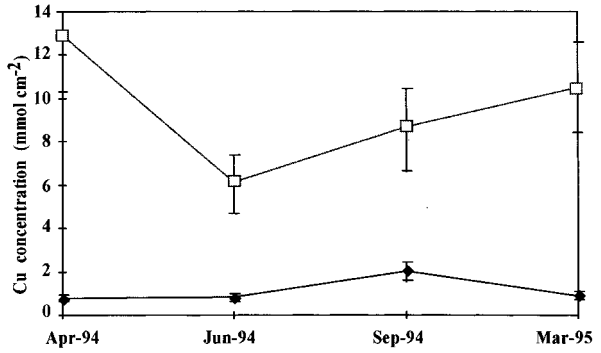

FIGURE 5. Integrated mass (top 10 cm) of HCl + HNO_3 Cu at site M (open squares) and at site S (solid circles).

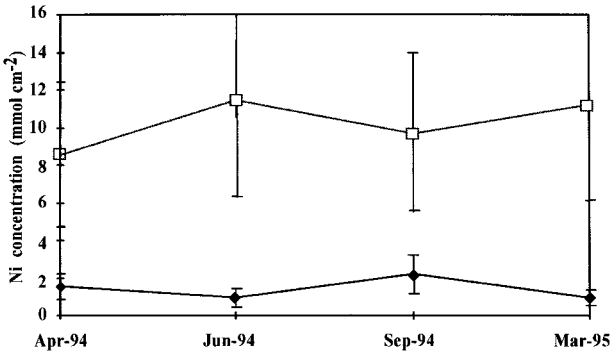

FIGURE 6. Integrated mass (top 10 cm) of HCl + HNO_3 Ni at site M (open squares) and site S (solid circles).

initial concentration of approximately 0.8 mmol cm^{-2} (Cu) and 8 mmol cm^{-2} (Zn) by March. Comparatively, HCl plus HNO_3 Hg did not vary appreciably (average concentration $\sim 6.6 \times 10^{-4}$ mmol cm^{-2}), and there is the potential for a seasonal maximum of approximately 2.2 mmol cm^{-2} for HCl plus HNO_3 Ni in October (Figure 7).

Site M (water depth ~12 m) is located in the mesohaline region of Chesapeake Bay where seasonal anoxia occurs in summer (*18*) and is representative of a sulfide-dominated environment. Depth-integrated (top 10 cm) AVS varied between 3.5 and 5.5 mmol cm^{-2} (Figure 3), and pyrite-S ranged from 7.5 to 10 mmol cm^{-2} (Figure 4). The sediments were fine-grained (porosity ~0.85) organic carbon comprised greater than 2.5% of total sediment mass, and greater than 40% of the HCl-extractable iron was associated with AVS minerals (Figure 2).

Published data on solid phase sulfur speciation within the same region as our study (*19*) agrees well with our observations of seasonal variability at site M, and values for

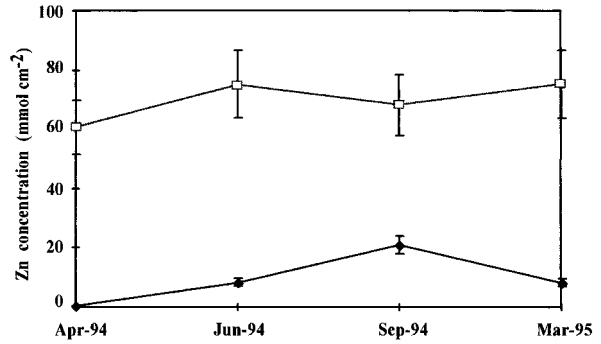

FIGURE 7. Integrated mass (top 10 cm) of HCl + HNO_3 Zn at site M (open squares) and site S (solid circles).

pore water sulfide and sulfate reduction rate (*16*, *19*) support our contention that site M is sulfide dominated. AVS and HCl Fe (Figure 3) displayed minimal seasonal variation (Figure 3). Pyrite-S (Figure 4) increased slightly from 7.6 mmol cm^{-2} (April) to 10.1 mmol cm^{-2} (June) and then decreased back to 8 mmol cm^{-2} for the remainder of the sampling period. Interestingly, HNO_3 Fe is at a minimum in June and then slowly increases through the remainder of the sampling periods. This discrepancy could indicate a sudden oxidation event (e.g., storm) that oxidizes pyrite and other sulfide minerals to produce Fe(II) and elemental sulfur (which extracts as pyrite-S). No seasonal trend was observed in the sum of HCl and HNO_3 metal for Cu (Figure 5), Ni (Figure 6), Zn (Figure 7), and Hg (data not shown, average concentration $\sim 3.1 \times 10^{-3}$ mmol cm^{-2}).

Discussion

Our data indicate that there is a direct link between the speciation of iron among sulfide and oxide minerals and the seasonal variability in the flux of total dissolved Cu from the sediments. Site S, which displays a distinct seasonality in the flux of total dissolve Cu and no seasonality in the flux of total Cu-complexing ligands from the sediments, is a sandy, bioturbated system where a large proportion of the "reactive" iron is present as oxide minerals. Site M, which displays a distinct seasonality in the flux of total Cu-complexing ligands but no seasonality in the flux of total dissolved Cu, is a silty, diffusion-dominated system where a large proportion of reactive iron is present as sulfide minerals. Both sites are subject to large seasonal shifts in bottom water temperature (*16*), DOC flux (*17*), $\sum CO_2$ flux (*17*), and sulfate reduction rate (*16*, *19*). Results from sediment analyses indicate that shifts in the iron−sulfur speciation at site S result in concomitant shifts in sediment metal concentrations, whereas shifts in iron−sulfur speciation at site M do not affect sediment metal concentrations. The agreement between sediment and water data combined with the dichotomy between site M and site S indicates that the dominant diagenetic processes controlling trace metal chemistry at site M are fundamentally different from those at site S. If this difference in metal chemistry is related to differences in iron−sulfur speciation, then the proportion of HCl-soluble iron associated with AVS minerals (%AVS-Fe) may be an easy-to-measure indicator of the chemical nature of the system.

In order to suggest directions for future research, we briefly present a general theory that relates metal chemistry to general iron−sulfur speciation. When aqueous sulfide reacts with aqueous iron (*20*, *21*) or directly with metastable iron oxyhydroxides (e.g., goethite, leipidocrocite) to form solid FeS (*22*), any trace metals that are released by these processes may complex strong ligands (e.g., organic matter), coprecipitate with iron sulfides, or adsorb to the surface of existent pyrite and AVS minerals. Continued dissolution of metastable iron oxyhydroxides, combined with the low solubility

of iron sulfide (mackinawite $K_{sp} \sim 3 \times 10^{-4}$), will lead to elevated concentrations of aqueous iron and very low concentrations of aqueous sulfide. These conditions will prevail until all sources of metastable iron oxyhydroxides have been exhausted, potentially allowing for a greater degree of metal-ligand formation, decreasing the net anion exchange between solid FeS and adsorbed trace metals (*6*), and inhibiting coprecipitation of trace metal sulfides with AVS minerals. Additionally, the lack of aqueous sulfide may increase the residence time of oxygen transported into the anoxic regime (*23*) and make solid phase sulfide more susceptible to oxidation reactions.

Without a sufficient supply of oxidants, continued sulfate reduction will ultimately exhaust a finite supply of metastable iron oxyhydroxides; increase the proportion of HCl-soluble Fe that is associated with AVS minerals; and eventually lead to an increase in the concentration of aqueous sulfide. This type of environment would result in a sulfide-dominated system where higher concentrations of aqueous sulfide inhibit metal-ligand formation, favor the formation of metal sulfide minerals, and allow rapid pyrite formation to sequester trace metals within pyrite via the reaction of FeS with aqueous polysulfide (*24*) or H_2S (*25, 27*). By reducing the residence time of oxygen in the sediments (*23*), high concentrations of aqueous and solid sulfide in the sulfide-dominated system could also "buffer" any potential oxidative dissolution of FeS(s) and help preserve trace metals that are associated with AVS minerals and pyrite.

The utility of %AVS-Fe as a proxy for system instability with respect to sulfide-associated metals is based on the observation (*27*) that the HCl extraction method used in this study (and most others) does not effectively separate iron oxide minerals according to their chemical reactivity during early diagenesis and the assertion that metals which are simply adsorbed to the surface of AVS minerals (potentially favored in Fe-dominated systems) will have different reaction kinetics than metals co-precipitated within the AVS matrix (potentially favored in S-dominated systems). Differences in the rate of sulfidization of the various iron oxide minerals (*28, 29*) will make the degree of sulfidization of these minerals (and the concentration of pore water sulfide) dependent upon the sulfate reduction rate as well as the concentration and distribution of iron oxide minerals. The percentage of highly reactive (HCl-soluble) iron that can be accounted for with an AVS analysis is a measure of the degree of sulfidization of the oxide minerals and reflects the potential for the presence of measurable pore water sulfide. Consequently, a large ratio of "sulfidized" to "oxidized" iron indicates a depositional environment where the supply of sulfide exceeds the supply of reactive oxidant (e.g., molecular oxygen, aqueous Fe^{3+}, metastable solid phase Fe^{3+}) and a small ratio of sulfidized to oxidized iron reflects the opposite.

In summary, our observations indicate that the nature of metal interactions with sulfide minerals is largely determined by the diagenetic environment. In sulfide-dominated environments, sulfide minerals can efficiently trap certain trace metals and inhibit the re-release of these metals to the overlying water. Trace metals may be released during major oxidation events, but (based on sedimentary metal and sulfur data) their residence time in the water column is probably less than 1 month. In iron-dominated systems, the sediments demonstrate a source-sink behavior with respect to sulfide minerals and associated trace metals, and there is less aqueous sulfide available to potentially inhibit metal-ligand formation. The formation of Fe- and S-dominated environments stems from the balance between sulfide production and the supply of reactive iron. Shifts in the magnitude of these two processes will lead to concomitant changes in iron–sulfur speciation and may ultimately affect trace metal speciation and subsequent diagenetic reactivity. Consequently, the key factors for predicting trace metal reactivity in an aquatic sedimentary environment are the potential for sulfide minerals to trap aqueous metals and inhibit metal-ligand formation and the potential for these same sulfide minerals to be destroyed via oxidative dissolution at a later date. Because the relative proportions of HCl-soluble iron and AVS can be indicative of important differences in sediment geochemistry, the ratio of reactive iron to AVS may present an inexpensive and useful indicator for the potential reactivity of sulfide minerals and associated trace metals within marine sediments.

Acknowledgments

We thank D. Burdidge, J. Donat, and S. Skrabal for their help collecting cores from Chesapeake Bay; J. Kovaks, P. Cheeseman, A. Schorlemmer, G. Chacko, T. S. Rhee, and B. Taylor for their invaluable contributions in the laboratory; Dr. Mandy Joye, Associate Editor Jerald L. Schnoor, and the anonymous reviewers whose comments have contributed greatly to this work. This work was funded by the Office of Naval Research, Marine Environmental Quality Program, and the Texas Sea Grant Program.

Literature Cited

(1) Davies-Colley, R. J.; Nelson, P. O.; Williamson, K. J. *Environ. Sci Technol.* **1984**, *18*, 491.
(2) Jacobs, L.; Emerson, S.; Skei, J. *Geochim. Cosmochim. Acta* **1985**, *49*, 1433.
(3) Skei, J. M.; Loring, D. H.; Rantala, R. T. T. *Mar. Chem.* **1988**, *23*, 269.
(4) Huerta-Diaz, M. A.; Morse, J. W. *Geochim. Cosmochim. Acta* **1992**, *56*, 2681.
(5) Di Toro, D. M.; Mahony, J. D.; Hansen, D. J.; Scott, K. J.; Hicks, M. B.; Mayr, S. M.; Redmond, M. S. *Environ. Toxicol. Chem.* **1990**, *9*, 1487.
(6) Di Toro, D. M.; Mahony, J. D.; Hansen, D. J.; Scott, K. J.; Carlson, A. R.; Ankley, G. T. *Environ. Sci. Technol.* **1992**, *26*, 96.
(7) Evangelou, V. P.; Zhang, Y. L. *Crit. Rev. Environ. Sci. Technol.* **1995**, *25*, 141.
(8) Morse, J. W. *Mar. Chem.* **1994**, *46*, 1.
(9) Morse, J. W. In *The Environmental Chemistry of Sulfide Oxidation*; Alpers, C. N., Blowes, D. W., Eds.; American Chemical Society: Washington, DC, 1994; Chapter 20.
(10) Cooper, D. C.; Morse, J. W. *Estuaries* **1996**, *19*, 595.
(11) Morse, J. W.; Cornwell, J. C. *Mar. Chem.* **1987**, *55*, 69.
(12) Canfield, D. E.; Raiswell, R.; Westrich, J. T.; Reaves, C. M.; Berner, R. A. *Chem Geol.* **1986**, *54*, 149.
(13) Huerta-Diaz, M. A.; Morse, J. W. *Mar. Chem.* **1990**, *29*, 119.
(14) Lord. C. J. *J. Sed. Pet.* **1982**, *52*, 664.
(15) Hatch, W. R.; Ott, W. L. *Anal Chem.* **1968**, *40*, 2085.
(16) Marvin-DiPasquale, M. C.; Capone, D. G. Submitted to *Mar. Ecol. Prog. Ser.*
(17) Skrabal, S. A.; Donat, J. R. *Limnol. Oceanogr.* In press.
(18) Burdidge, D. J.; Homstead, J. *Geochim. Cosmochim. Acta* **1994**, *58*, 3407.
(19) Roden; Tuttle. *Mar. Ecol. Prog.* **1993**, *93*, 101.
(20) Rickard, D. T. *Am. J. Sci.* **1974**, *274*, 941.
(21) Rickard, D. T. *Geochim. Cosmochim. Acta* **1995**, *59*, 4367.
(22) Peiffer, S.; Afonso, M. S.; Wehrll, B.; Gachter, R. *Environ. Sci. Technol.* **1992**, *26*, 2408.
(23) Morgan, J. J. *Environ. Sci. Technol.* **1980**, *14*, 183.
(24) Luther, G. W. *Geochim. Cosmochim. Acta* **1991**, *55*, 2839.
(25) Rickard, D. T. *Geochim. Cosmochim. Acta* **1996**, *61*, 115.
(26) Rickard, D. T.; Luther, G. W. *Geochim. Cosmochim. Acta* **1996**, *61*, 135.
(27) Kostka, J. E.; Luther, G. W. *Geochim. Cosmochim. Acta* **1994**, *58*, 1701.
(28) Canfield, D. E.; Raiswell, R.; Bottrell, S. *Am. J. Sci.* **1992**, *292*, 659.
(29) Raiswell, R. *Chem. Geol.* **1993**, *107*, 467.

Received for review May 1, 1997. Revised manuscript received November 3, 1997. Accepted November 10, 1997.

ES970387E